Structural Sizing of Wing Spar in Fixed-Wing Unmanned Aerial Vehicle Concept Using Tsai-Hill Failure Criterion

Hariel Dumont Dias Sousa[1*], Jefferson dos Reis do Carmo[1], Mateus Baqueiro Mendonça O'Dwyer[1], Kauan Dantas Brito da Silva[1], Guilherme Prazeres Matos de Souza[1], Douglas Lima Silva[2], Bruno de Sousa Silva[2]

[1]SENAI CIMATEC University, Center of Competence in Aeronautical Engineering and Drones; [2]SENAI CIMATEC University, Department of Industrial Product Development; Salvador, Bahia, Brazil

The structural design for a Fixed-Wing Unmanned Aerial Vehicle (UAV) begins with preliminary aeronautical calculations driven by the mission profile. This profile defines key requirements such as endurance, cruise altitude, and payload capacity, which in turn guide the estimation of gross weight, wing loading, and power-to-weight ratio. These parameters determine the wing planform area, span, and aspect ratio, optimizing aerodynamic efficiency. Based on these definitions, wing load calculations are performed, accounting for distributed loads from lift and any concentrated loads from internal masses. Bending moment, shear force, and torsional moment diagrams along the span are obtained for the most critical load case. The results contribute to the subsequent structural design phase. With the maximum loads identified, the sizing of the stringers (longitudinal stiffeners installed along the wing skin). For this purpose, the reinforced shell model was adopted, composed of a core and flanges in polymer matrix composite material and fiber reinforcement, with assumptions of symmetry and linear loading. The stringers are sized to withstand buckling and axial compression, considering the maximum bending moment and the section centroid position. The cross-section of the profiles was selected based on the relationship between structural weight and stiffness. This process ensures that the structure withstands in-flight loads with minimum weight, applying the Tsai-Hill failure criterion. Using a numerical computing code to assess multiple geometries, the optimal configuration achieved reduced structural weight while maintaining an adequate minimum safety margin.

Keywords: UAV. Load Calculations. Structural Sizing. Stringers. Tsai-Hill.

Abbreviations: UAV, Unmanned Aerial Vehicle.

In the conceptual design phase of an aircraft, aerodynamics guides critical decisions such as the selection of the airfoil profile, the definition of fuselage geometry, and the configuration of control surfaces. In his study, Raymer [1] concludes that these elements directly influence the lift, drag, and moment coefficients, which are decisive for the aircraft's flight behavior and operational envelope. As Barros [2] states that performance targets are an essential part of aircraft design, the study of the aircraft structure becomes necessary to validate the conceptual design.

The main structural component of the wing is the spar, responsible for carrying bending, torsional, and distributed loads along the wingspan. Therefore, the present study aims to analyze the structural sizing of a wing spar in a Fixed-Wing Unmanned Aerial Vehicle (UAV) concept, applying the Tsai–Hill failure criterion.

Materials and Mtehods

The method was based on three main pillars: preliminary aeronautical calculations, wing load analysis, and main spar sizing. The structural assessment under critical conditions aims to determine key parameters such as deflection, torsion, ultimate loads, failure modes, load combinations, and life-cycle analysis. By understanding the structural behavior under variable loading conditions, it becomes possible to predict potential failure modes and define mitigation strategies, thereby contributing to the continuous improvement of the design.

Received on 15 October 2025; revised 10 January 2025.

Address for correspondence: Hariel Dumont Dias Sousa. Av. Orlando Gomes, 1845, Piatã, Salvador, Bahia, Brazil. Zipcode: 41650-010. E-mail: neon.951@hotmail.com.

J Bioeng. Tech. Health 2026;9(2):83-90

© 2026 by SENAI CIMATEC University. All rights reserved.

Preliminary Aeronautical Calculations

In his study, Raymer [1] defined that the initial phase of aircraft development is driven by the mission concept, which determines the key design decisions. In this context, the mission serves as the guiding factor for preliminary aeronautical calculations. As a case study, a UAV designed for coastal surveillance was considered, defining its baseline geometry as well as aerodynamic and propulsion characteristics.

Through benchmarking, existing UAV designs with similar mission requirements were analyzed in order to establish performance targets and structural parameters. The initial parameters for the aeronautical calculations were set based on standard and commercially available values for UAVs with comparable operational profiles.

For Raymer [1], the actual empty weight will be calculated by estimating and summing the weights of all aircraft components. Based on this, initial estimates for Maximum Takeoff Weight (MTOW), empty weight, and payload capacity were carried out. The basic dimensions (wing area, wingspan, and fuselage length) were estimated using data from similar aircraft, along with parameters such as wing loading, aspect ratio, and thrust-to-weight ratio. These were used to analyze the constraint diagram, correlating thrust-to-weight and wing loading to determine the feasible wing area and preliminary power requirements for the project.

Given that the intended mission is surveillance, the operational goal is to maximize endurance, following the methodology derived from the Breguet endurance equation, according to Raymer [1].

Wing Load Calculations

For the definition of limit loads, the method described in Barros [2] was adopted, based on JAR-VLA 333 [3]. Initially, a free-body diagram was developed to map all forces and moments acting on the UAV during steady, level flight, as shown in Figure 1. The diagram includes thrust force (T), drag force (D), weight force (W), wing lift force (Lw), vertical stabilizer lift force (Lev), horizontal stabilizer lift force (Lht), moment generated by wing lift (Mw), and the moment generated by horizontal stabilizer lift and the aerodynamic center (AC).

Subsequently, a flight envelope, also known as a V–n diagram, was developed to define the operational limits of the aircraft. The envelope consists of both maneuver and vertical gust diagrams. By developing the maneuver diagram, it was possible to determine the operating speeds, including stall speed (VS), maneuvering speed (VA), cruise speed (VC), and dive speed (VD), following the JAR-VLA 335 [4] reference. However, due to the absence of a defined propulsion system, the maximum speed was determined based on the legal limit for UAVs

Figure 1. Free-body diagram of a UAV.

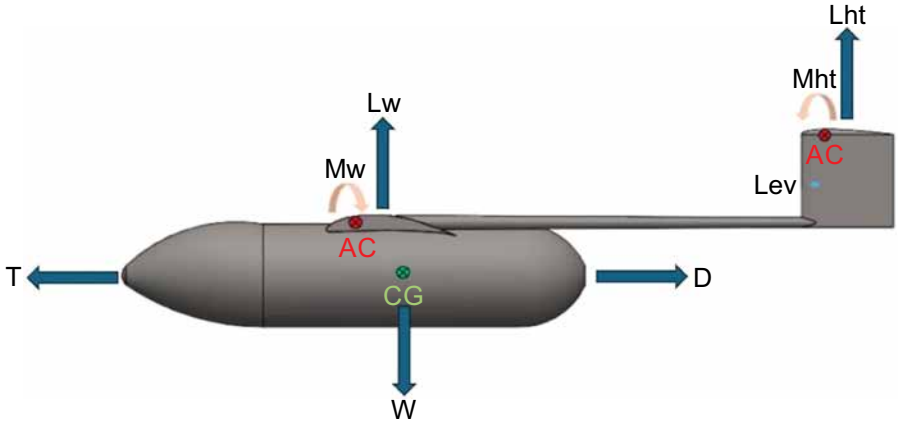

in Brazil, according to DECEA's AC100-40 [5], corresponding to 33.33 m/s.

The maximum (nmax) and minimum (nmin) load factors were initially defined in accordance with JAR-VLA 337 [6]. However, since this regulation was intended for manned aircraft, the prescribed values did not meet the design requirements. Therefore, based on the method described in Rosa [7], the nmax and nmin values were adjusted to better suit the project specifications. Table 1 presents the values used for the development of the maneuver diagram.

For the development of the vertical gust diagram, several factors influencing the forces acting on the aircraft throughout all phases of flight were considered. Among these forces, the gust load stands out, characterized by sudden and temporary changes in velocity that can lead to increased structural loads due to abrupt variations in dynamic pressure, according to Raymer [1].

The study focused exclusively on strictly vertical gusts, as they directly influence the increase or decrease of the load factor. According to JAR-VLA 341 [8], gust loads must be calculated using a gust gradient (Ude) of 15.24 m/s. However, since this standard was primarily intended for analyses of commercial aircraft, adopting this value would result in an overly conservative V-n diagram, leading to an unnecessarily robust and heavy UAV.

Nevertheless, NACA Report NR-692 [9] indicates that, for altitudes below 1,066.8 meters, gust velocities do not exceed 7.62 m/s, with over 95% of recorded measurements being below 6.10 m/s. The report also provided gust gradient (Ude) data as a function of altitude, allowing interpolation and derivation of equations.

Therefore, to define the parameters, a reference altitude of 150 meters and an operational radius of 30 km were adopted. As a result, Ude was determined as 8.06 m/s for cruise speed (VC) and 4.03 m/s for dive speed (VD). Subsequently, the calculation of positive and negative gust-induced load factors (ngust+ and ngust–) and their respective parameters was carried out following the procedures described in JAR-VLA 341 [8]. The obtained values are presented in Table 2.

Upon completion of the diagrams, a provisional V-n diagram (using estimated values) could be developed, serving as a guide for all load analysis and simulation processes. The diagram is illustrated in Figure 2.

For proper structural sizing, a load combination analysis must be performed based on individually calculated load effects. This study was essential because, during flight, the UAV will be subjected to loads that generate various combined forces, such as shear forces, bending moments, and torsional moments at a single point. Gust-induced loads must be analyzed separately, without the influence of other load effects. After selecting the critical cases from the flight envelope, the acting loads and moments for each selected condition could be extracted.

For this purpose, the method of Barros [2] was followed, which employs the Stender chord method. This method was based on the aerodynamic lift distribution and wing geometry to estimate the resulting internal loads. The analysis of all cases within the V-n diagram and the extraction of their

Table 1. Parameters for the maneuvering diagram.

Symbol	Definition	Value	Value
VS	Stall speed	11.84 m/s	42.62 km/h
VC	Cruise speed	30.00 m/s	108.00 km/h
VD	Dive speed	37.50 m/s	135.00 km/h
VA	Maneuvering speed	20.51 m/s	73.83 km/h
nmax	Maximum load factor	3.00	-
nmin	Minimum load factor	-1.00	-

Table 2. Parameters for the gust diagram.

Symbol	Definition	Value [-]
ug	Aircraft mass ratio	11.4367
Kg	Gust alleviation factor	0.6013
ngust + VC	Load factor due to positive gust at VC	5.9005
ngust - VC	Load factor due to negative gust at VC	-3.9005
ngust + VD	Load factor due to positive gust at VD	4.0628
ngust - VD	Load factor due to negative gust at VD	-2.0628

Figure 2. Provisional V-n diagram.

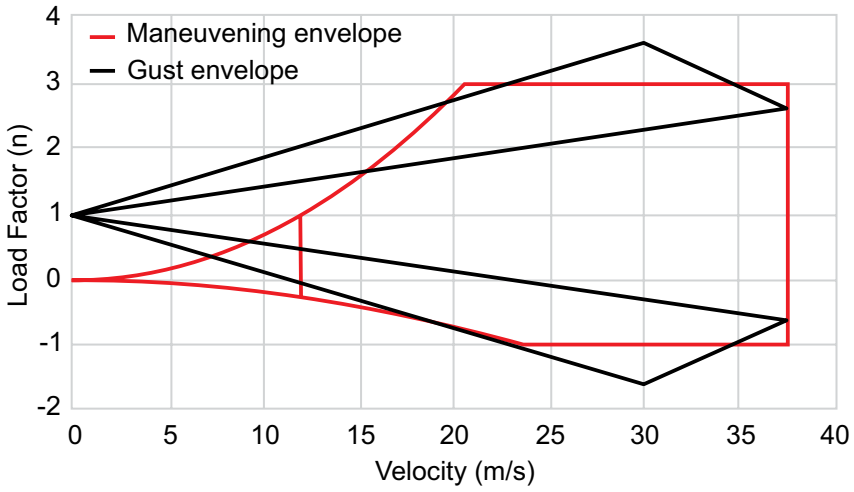

corresponding limit loads was of utmost importance, as they guide the aircraft's structural sizing.

The design safety factor (FOS) is a coefficient applied conservatively to assist in the UAV structural design. Structures must be designed to withstand loads multiplied by the safety factor, ensuring robustness beyond expected operational conditions. The safety factor adopted for the UAV structural design is defined as 1.5 to provide limited safety margins, in accordance with JAR-VLA 303 [10] standard.

Ultimate Loads are obtained by multiplying Limit Loads by the safety factor. They represent the maximum load that the structure can sustain before failure and are used in structural testing for verification and validation purposes. These ultimate loads were applied throughout the entire semi-wingspan and, at the end of the analysis, Table 3 presents the Ultimate Loads based on the highest loads found.

With this study completed, the detailed structural design process can begin, considering the identified critical loads.

Sizing of the Stringer

Tahir [11], in his study, addresses the Failure Criterion as being used to evaluate the structural capacity to support a given load, regardless of

Table 3. Ultimate loads based on the highest limit loads found.

Type of Load	Limit Loads	FOS	Ultimate Loads
Shear Force	585 N	1.5	877.5 N
Bending Moment	573 N.m	1.5	859.5 N.m
Twisting Moment	142 N.m	1.5	213 N.m

the occurrence of failure. The Tsai-Hill failure theory is an adaptation of the Von Mises theory for applications in anisotropic materials, such as unidirectional composite laminates. It considers the interactions between the stress components in the blade, allowing failure prediction based on distortion energy, according to Talreja [12]. Therefore, this criterion was employed to guide the preliminary sizing of the wing spar, as represented by Equation 1.

$$\left(\frac{\sigma_1}{X}\right)^2 - \left(\frac{\sigma_1 \cdot \sigma_2}{X^2}\right) + \left(\frac{\sigma_2}{Y}\right)^2 + \left(\frac{\tau_{12}}{S}\right)^2 \leq 1 \quad (1)$$

In the case where the left-hand term, also known as the Tsai-Hill index, is less than or equal to 1, the developed structure can withstand the loads. If the term is greater than 1, failure will occur. This criterion considers the interaction between normal and shear stresses, being simple for application in initial design simulations and providing an approximate elliptical failure envelope, which would be useful for preliminary safety assessments.

For the spar, a box configuration was selected because it distributes more material away from the neutral axis, and consequently provides greater bending resistance. The cross-section was divided into two parts, as shown in Figure 3.

For the determination of the properties required in the calculation of the Tsai-Hill index, a study of strength of materials was necessary. In the geometric property of an area, the centroid is analyzed, which refers to the point that defines its geometric center, as defined by Hibbeler [13]. To determine the area moment of inertia of the hollow rectangular section, used in bending analysis, Equation 2 was applied, based on Hibbeler [13].

$$I = \frac{\left(B \cdot H^3 - b \cdot h^3\right)}{12} \quad (2)$$

For the torsion analysis, it was necessary to calculate the polar moment of inertia of the hollow rectangular section, as represented in Equation 3, expressed by Hibbeler [13].

$$J = \frac{(B \cdot H^3 - b \cdot h^3)}{12} + \frac{(H \cdot B^3 - h \cdot b^3)}{12} \quad (3)$$

For Hibbeler [13], the safety factor was used to ensure that structural elements operate within acceptable stress limits, providing a margin against unexpected failures due to variations in materials, loads or operating conditions.

In this project, a wing with a semi-span of 2.33 m was considered, subjected to a distributed load along the span, representing the aerodynamic load generated during flight. To increase the analysis resolution, the load was discretized into 100 equally spaced points, allowing calculation of the bending moment and torque at each section along the wing.With the definition of the moments of inertia, it was possible to calculate the normal

Figure 3. Spar cross-sections.

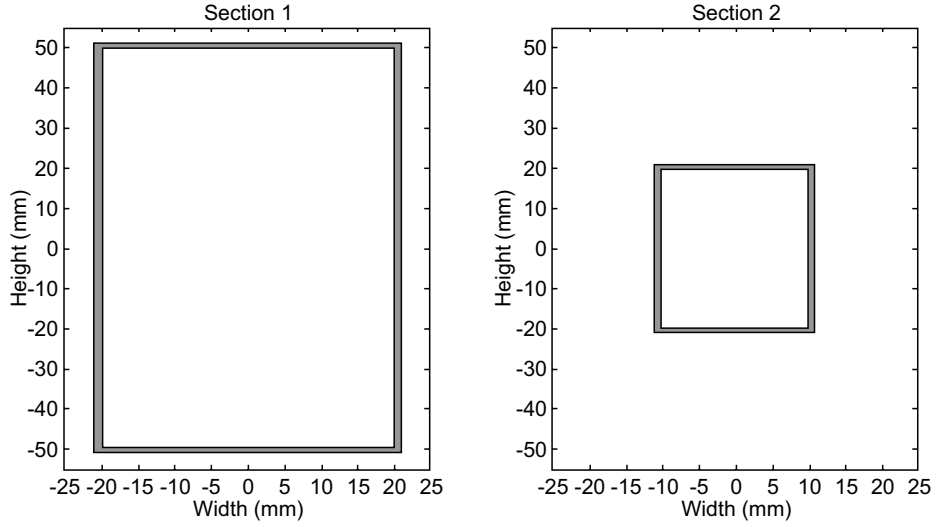

stress due to bending and the shear stress due to torsion, expressed by Hibbeler [13]. The formulas are represented in Equations 4 and 5, respectively.

$$\sigma = \frac{M_f \cdot \left(\frac{D}{2}\right)}{I} \cdot 10^{-6} \quad (4)$$

$$\tau_{max} = \frac{M_t \cdot \left(\frac{D}{2}\right)}{J} \cdot 10^{-6} \quad (5)$$

For the calculation of the Tsai-Hill index, it was necessary to determine the in-plane principal stresses and the maximum in-plane shear stress. The principal stresses correspond to the maximum and minimum normal stress values that occur at a point, on planes where the shear stress is zero. The maximum shear stress represents the highest absolute value that the shear stress can reach on any plane passing through that point. In his study, Timoshenko [14] uses Mohr's circle, which is a graphical tool that allows visualizing the plane stress state, providing intuitively and accurately the values of the principal stresses and the maximum shear stress, expressed by Hibbeler [13].

The principal stresses and maximum shear stress are determined from Equations 6 and 7, respectively.

$$\sigma_{1,2} = \frac{\sigma}{2} \pm \sqrt{\left(\frac{\sigma}{2}\right)^2 + \tau_{max}^2} \quad (6)$$

$$\tau_{12} = \frac{\sigma_1 - \sigma_2}{2} \quad (7)$$

A numerical computing software code was developed to perform the Tsai-Hill methodology calculations. After various geometry combinations, it was possible to find an optimum point for weight and acceptable safety margin. The geometries are represented in Figure 4.

For the determination of materials and their respective properties, a benchmark was conducted focusing on UAVs with similar mission profiles and geometry. Due to market trends and high structural efficiency, carbon fiber reinforced plastic (CFRP) was defined as the sole material to comprise the spar. To determine the properties, the research by Santos [15] and the datasheet from Toray Carbon Fibers Europe [16] were used. The properties utilized are presented in Table 4.

Results and Conclusion

The results obtained allow the selection of cross-sectional configurations that minimize structural weight while maintaining the failure index below 1, respecting operational limits.

By applying the Tsai-Hill method to this geometry, a positive safety margin curve was obtained, with the minimum safety margin equal to 34.49%, located at the wing root semi-span. Using the bending moment equation, it was possible to determine the deflection along the semi-span through direct integration. It was also possible to find the twist angle along the span through double integration of the torsional moment. Therefore, a maximum deflection of 123.66 mm was obtained,

Figure 4. Final geometry of cross-sections.

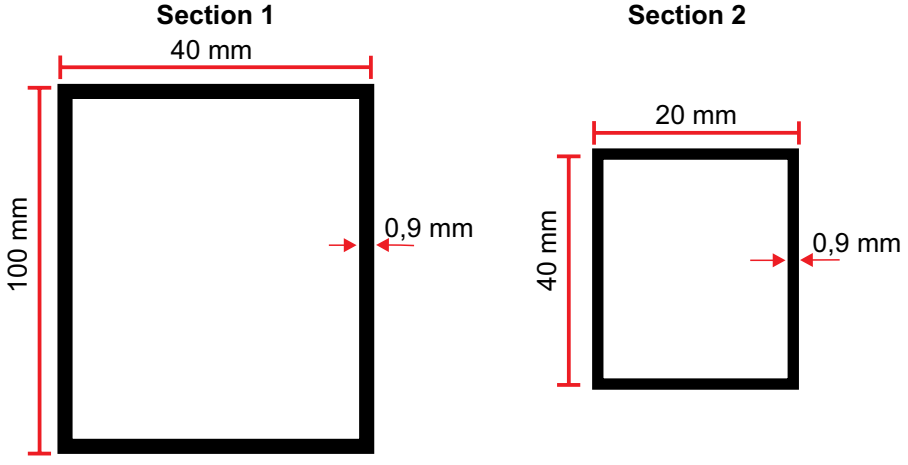

located at the wing tip, and a maximum twist of 12.7°. These values are positive since they represent deformation values that do not considerably alter the aerodynamic properties of the design. The results are presented in Figure 5.

Subsequently, it was possible to calculate the estimated weight of the spar based on the density and volume of carbon fiber used, resulting in 0.982 kg.

The study demonstrates the feasibility of using the Tsai-Hill criterion as a reliable tool in the initial phases of UAV structural design, contributing to the development of lightweight, efficient, and safe aircraft.

Figure 5. Final charts of sizing indicators.

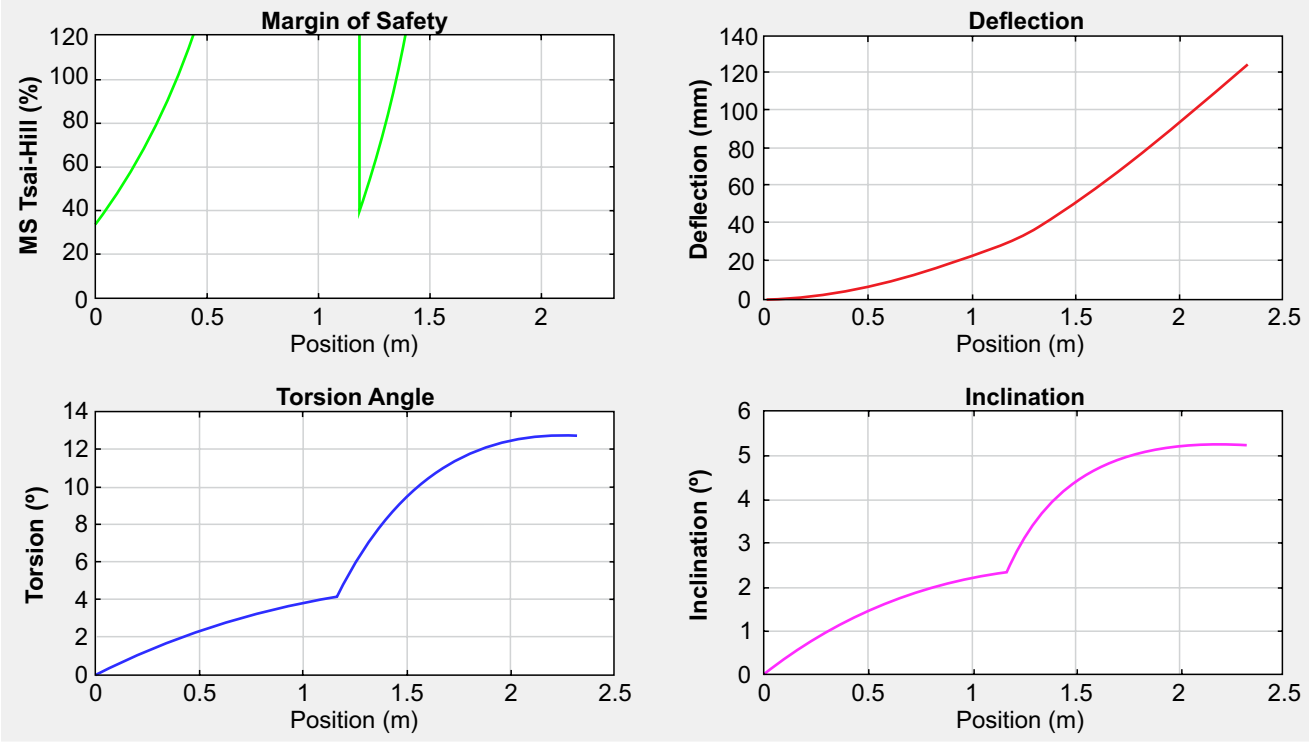

References

1. Raymer DP. Aircraft design: a conceptual approach. 6th ed. Reston: American Institute of Aeronautics and Astronautics; 2018.
2. Barros CP. Introdução ao projeto de aeronaves leves. Belo Horizonte: Centro de Estudos Aeronáuticos (CEA), UFMG; 2001.
3. United States. Federal Aviation Administration (FAA). Title 14 – Aeronautics and Space: Part 23, § 23.333 – Flight envelope. Washington (DC): U.S. Government Publishing Office; 2025.
4. United States. Federal Aviation Administration (FAA). Title 14 – Aeronautics and Space: Part 23, § 23.335 – Design airspeeds. Washington (DC): U.S. Government Publishing Office; 2025.
5. Brazil. Airspace Control Department (DECEA). Instruction of the Air Force Command (ICA) 100-40: Unmanned aircraft and access to Brazilian airspace; 2023.
6. United States. Federal Aviation Administration (FAA). Title 14 – Aeronautics and Space: Part 23, § 23.337 – Limit maneuvering load factors. Washington (DC): U.S. Government Publishing Office; 2025.
7. Rosa E. Introdução ao projeto aeronáutico: uma contribuição à competição SAE AeroDesign. Florianópolis: UFSC/Grante; 2006.
8. United States. Federal Aviation Administration (FAA). Title 14 – Aeronautics and Space: Part 23, § 23.341 – Gust load factors. Washington (DC): U.S. Government Publishing Office; 2025.
9. National Advisory Committee for Aeronautics (NACA). Effective gust structure at low altitudes as determined from the reactions of an airplane. NACA Report No. 692; 1940.

10. United States. Federal Aviation Administration (FAA). Title 14 – Aeronautics and Space: Part 23, § 23.303 – Factor of safety. Washington (DC): U.S. Government Publishing Office; 2025.
11. Tahir NM, Alhaji AU, Abdullahi I. Performance evaluation of unmanned aerial vehicle wing made from Sterculia setigera fiber and Pterocarpus erinaceus wood dust epoxy composite using finite element method Abaqus and structural testing. Res Eng Struct Mater. 2022;8(4):675-694. doi:10.17515/resm2022.378ma0102tn.
12. Talreja R. Assessment of the fundamentals of failure theories for composite materials. Compos Sci Technol. 2014;105:190-201. doi:10.1016/j.compscitech.2014.10.014.
13. Hibbeler RC. Resistência dos materiais. 7th ed. São Paulo: Pearson Prentice Hall; 2009.
14. Timoshenko SP, Gere JM. Theory of elastic stability. 2nd ed. Boston: McGraw-Hill; 1961.
15. Santos CPS, Bichara JRR. Estudo experimental das propriedades mecânicas para compósito em fibra de carbono e matriz epóxi Pipefix (CFRP – Carbon Fiber Reinforced Polymer). Rio de Janeiro: CEFET-RJ; 2015. Available from: https://www.cefetrj.br/attachments/article/2943/Estudo_Experimental_Propriedades_Mec_Comp%C3%B3sitos_Fibra_Carbono_e_Matrix_Ep%C3%B3xi_Pipefix.pdf
16. Toray Carbon Fibers Europe. Torayca M60J: technical data sheet [Internet]. 2025. Available from: https://toray-cfe.com/wp-content/uploads/2025/02/Torayca-M60J-Technical-Data-Sheet.pdf